



A novel microscopy-based assay identifies extended synaptotagmin-1 (ESYT1) as a positive regulator of anoctamin 1 traffic



Joana R. Lérias^{a,b,1}, Madalena C. Pinto^{a,b,c,1}, Hugo M. Botelho^a, Nikhil T. Awatade^a, Margarida C. Quaresma^a, Iris A.L. Silva^a, Podchanart Wanitchakool^b, Rainer Schreiber^b, Rainer Pepperkok^c, Karl Kunzelmann^b, Margarida D. Amaral^{a,c,*}

^a University of Lisboa, Faculty of Sciences, BioISI - Biosystems & Integrative Sciences Institute, Campo Grande, C8, 1749-016 Lisboa, Portugal

^b Department of Physiology, University of Regensburg, Universitätsstrasse 31, 93053 Regensburg, Germany

^c Cell Biology and Biophysics Unit and Advanced Light Microscopy Facility, European Molecular Biology Laboratory (EMBL), Meyerhofstraße 1, 69117 Heidelberg, Germany

ARTICLE INFO

Keywords:

Intracellular traffic
Endoplasmic reticulum
Calcium-activated chloride channels
Cystic fibrosis
Automated fluorescence microscopy

ABSTRACT

An attractive possibility to treat Cystic Fibrosis (CF), a severe condition caused by dysfunctional CFTR, an epithelial anion channel, is through the activation of alternative (non-CFTR) anion channels. Anoctamin 1 (ANO1) was demonstrated to be a Ca²⁺-activated chloride channel (CaCC) and thus of high potential to replace CFTR. Despite that ANO1 is expressed in human lung CF tissue, it is present at the cell surface at very low levels. In addition, little is known about regulation of ANO1 traffic, namely which factors promote its plasma membrane (PM) localization.

Here, we generated a novel cellular model, expressing an inducible 3HA-ANO1-eGFP construct, and validated its usage as a microscopy tool to monitor for ANO1 traffic.

We demonstrate the robustness and specificity of this cell-based assay, by the identification of siRNAs acting both as ANO1 traffic enhancer and inhibitor, targeting respectively COPB1 and ESYT1 (extended synaptotagmin-1), the latter involved in coupling of the endoplasmic reticulum to the PM at specific microdomains. We further show that knockdown of ESYT1 (and family members ESYT2 and ESYT3) significantly decreased ANO1 current density.

This ANO1 cell-based assay constitutes an important tool to be further used in high-throughput screens and drug discovery of high relevance for CF and cancer.

1. Introduction

Cystic Fibrosis (CF) is the most common life-shortening (median age at death ~28 years) rare disease, affecting ~32,000 individuals in Europe (~85,000 worldwide). This inherited disease results from mutations in the gene encoding the CF transmembrane conductance regulator (CFTR), an epithelial chloride (Cl⁻) and bicarbonate (HCO₃⁻) anion channel. Despite symptomatic therapies, quality of life and life expectancy are still limited. Thus, correction of the CF basic defect, i.e., restoration of epithelial Cl⁻/HCO₃⁻ secretion through CFTR modulators, is the much ambitious alternative [1]. Despite some success in

getting to the clinic, CFTR modulators nevertheless cannot be used to pharmacologically rescue all CFTR mutations, e.g., large deletions such as the *del2,3*(21 kb) mutation, quite frequent in Slavic countries. For CF patients with these ‘unrescuable’ mutations, recently grouped into class (theratype) VII [2], the alternative is to develop ‘mutation-agnostic’ therapies. One such possibility is through the activation of alternative (non-CFTR) anion channels [3].

Anoctamins consist in a family of 10 different proteins, ANO1-10 (also known as TMEM16A-H, J and K, respectively), with some of its members reported to be (or to regulate) Cl⁻ channels. Indeed, Anoctamin 1 (ANO1) was identified as a calcium (Ca²⁺)-activated Cl⁻

Abbreviations: ANO, Anoctamin; BSA, bovine serum albumin; CaCC, calcium (Ca²⁺)-activated Cl⁻ channel; CF, cystic fibrosis; CFBE, cystic fibrosis bronchial epithelial (cells); CFTR, cystic fibrosis transmembrane conductance regulator; Dox, doxycycline; ER, endoplasmic reticulum; EGFR, epidermal growth factor receptor; ERQC, ER quality control; ESYT1, extended synaptotagmin-1; HA, hemagglutinin; HTS, high throughput screening; I_{sc}, short circuit current; PBS, phosphate buffered saline; PFA, paraformaldehyde; PM, plasma membrane; TEER, transepithelial resistance; V_{te}, transepithelial voltage; WB, Western blot

* Corresponding author at: University of Lisboa, Faculty of Sciences, BioISI - Biosystems & Integrative Sciences Institute, Campo Grande, C8, 1749-016 Lisboa, Portugal.

E-mail address: mdamaral@fc.ul.pt (M.D. Amaral).

¹ Equal contribution.

<https://doi.org/10.1016/j.bbamcr.2017.11.009>

Received 12 June 2017; Received in revised form 2 November 2017; Accepted 14 November 2017

Available online 15 November 2017

0167-4889/© 2017 Elsevier B.V. All rights reserved.

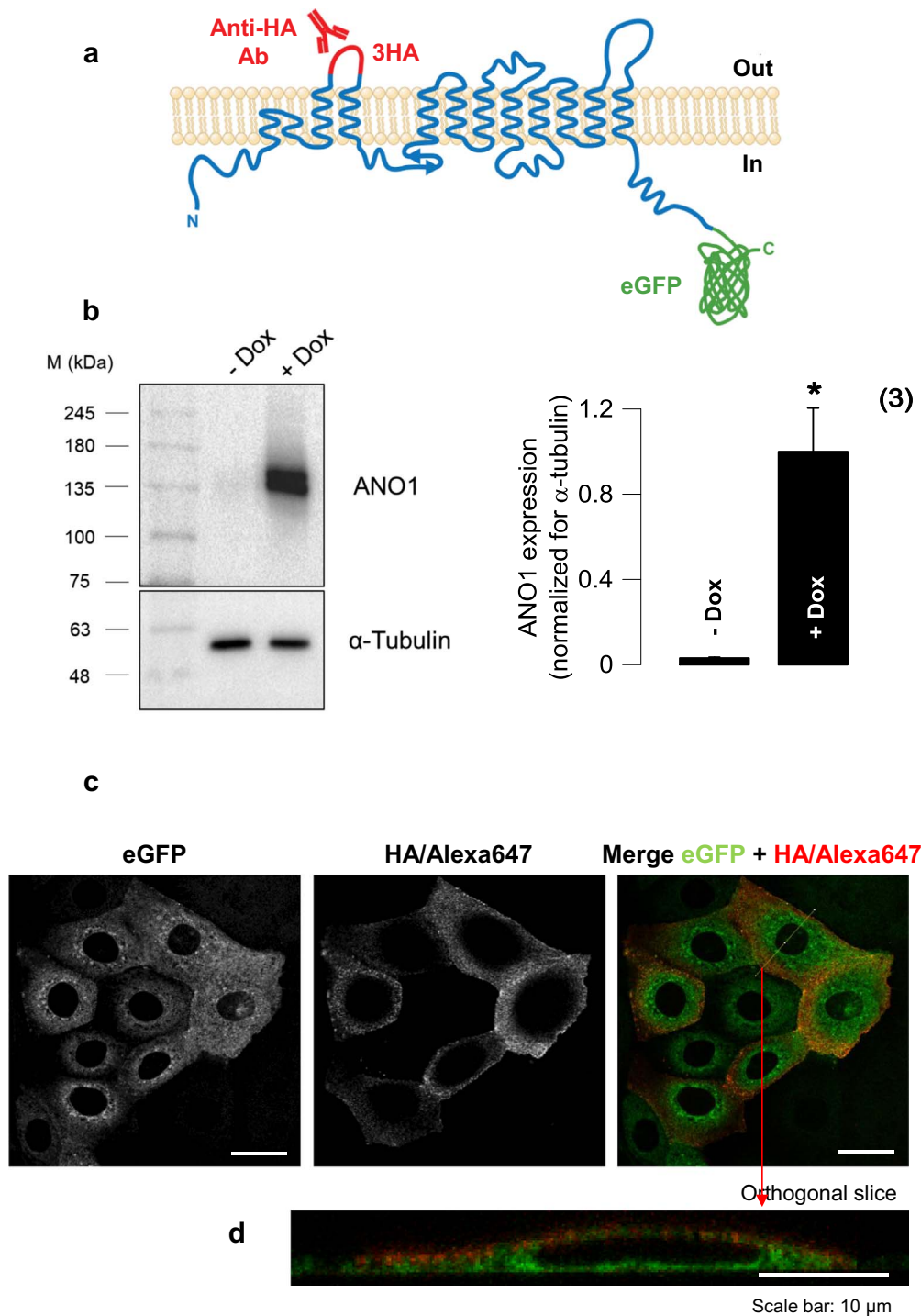


Fig. 1. Schematic representation of the 3HA-ANO1-eGFP traffic reporter construct and ANO1 expression levels and intracellular localization after induction. (a) Topology of the ANO1 protein showing the ten transmembrane domains. eGFP was fused to the C-terminus of ANO1 via a 17-amino acid linker sequence (Fig. S1). The triple hemagglutinin (3HA) tag was introduced in the first extracellular loop and becomes accessible to the extracellular space when the construct is inserted in the PM. Cells were grown in the presence of 1 μ g/ml Dox for 48 h so as to induce double-tagged ANO1 expression. (b) WB of 3HA-ANO1-eGFP CFBE cells non-induced (-Dox) or induced (+Dox) where ANO1 was detected by the primary antibody DOG1 (1:500) demonstrating the higher levels of ANO1 in induced vs non-induced cells and thus confirming ANO1-inducibility in this cell line. Endogenous protein is not detected since it is expressed at much lower levels. α -Tubulin was used as a loading control and molecular mass markers are shown on the left. (c) Images showing ANO1 expression and PM fraction in unpermeabilized CFBE cells. **Left panel:** total amount of expressed ANO1, represented by eGFP fluorescence. **Middle panel:** Alexa Fluor® 647 (immuno) fluorescence of anti-HA antibody detecting 3HA tags exposed extracellularly, i.e. ANO1 molecules present at the PM. **Right panel:** merged image of the two fluorescence channels: Green - eGFP, red - HA/Alexa 647. Images were acquired in Leica TCS SP8 confocal microscope (objective: 60 \times water, NA 1.4). Scale bar = 30 μ m. (d) Orthogonal slice (z plane) of a representative cell displayed where it is possible to confirm that the anti-HA antibody (HA/Alexa647) - represented in red - is staining only the PM subcellular localization of the 3HA-ANO1-eGFP CFBE cells. Scale bar = 10 μ m.

channel (CaCC) [4–6]. Also ANO2 was reported to be the CaCC mediating olfactory signal transduction [7] and ANO6 was identified as the main component of outwardly rectifying chloride channel (ORCC) [8]. However, ANO5, ANO7, ANO8, ANO9 and ANO10 do not appear to mediate ion transport [9,10]. Besides transepithelial ion transport, anoctamins were reported to also play a variety of physiological functions ranging from being Ca^{2+} -dependent lipid scramblases - ANO3,4,5,6,7,9 [11,12] - regulating other ion channels, to mediating smooth muscle contraction, olfaction, phototransduction, nociception, and control of neuronal excitability [9,10,13].

ANO1/TMEM16A has a fundamental importance for Ca^{2+} -dependent Cl^- secretion in various epithelia, namely in the airways, salivary

gland, pancreatic gland, and hepatocytes [14–16]. Indeed, in vivo siRNA knockdown of ANO1 resulted in reduced fluid secretion in salivary glands [16]. Importantly, native epithelia of mice with genetic ablation of ANO1/TMEM16A fail to generate Ca^{2+} -activated Cl^- transport, namely in the airways, and also evidence compromised mucociliary clearance with accumulation of mucus in the airways, in striking similarity to CF respiratory disease [14,15,17]. In addition to Cl^- , ANO1 was also shown to transport HCO_3^- after physiological stimulation [18,19], suggesting that this channel could also replace CFTR-mediated HCO_3^- transport. Altogether, these data demonstrate the important role of ANO1 in fluid secretion and make it an attractive candidate for novel treatments for CF to compensate for defective

CFTR-mediated anion transport.

Notwithstanding, we still miss essential knowledge on how to stimulate ANO1 independently of Ca^{2+} , an essential requirement for its potential pharmacological applications. Although ANO1 was reported to localize in the apical membrane of airway epithelial cells [17,20], it is present at the cell surface at low levels [17]. Moreover, little is known about regulation of ANO1 traffic, namely which factors promote its plasma membrane (PM) localization. Intriguingly, recent studies show that ANO1 can also play a tethering role of receptors, e.g., the inositol trisphosphate (IP_3) receptor - and endoplasmic reticulum (ER) Ca^{2+} stores to the PM [21]. According to this hypothesis, intracellular ANO1 (and possibly other ANO proteins) may not be the channels themselves, but instead mediate activation through coupling of Ca^{2+} signals of other membrane-localized channels [22]. Understanding how this regulation takes place is very relevant for human disease, since ANO1 was also reported to play a role in other diseases, namely various forms of cancer [23].

In any case, substantial knowledge is missing regarding the molecular basis of Ca^{2+} -dependent Cl^- transport by anoctamins, as we still lack key pieces of information on most basic aspects, like how (and whether) they traffic to the PM. Yet, this is a crucial aspect for a detailed molecular mechanism of ANO1 regulation or of its regulation of other channels. An outstanding question is thus under which conditions is ANO1 located intracellularly and what factors promote its PM localization.

Early studies on TMEM16A proposed the alternative name of anoctamin 1 since it exhibited selectivity for anions and was believed to have eight (oct-) transmembrane domains [4]. In fact, high-resolution structural analysis of the fungal homologue from the fungus *Nectria haematococca* nh TMEM16, revealed 10 instead of eight transmembrane domains [24] which was subsequently confirmed by a topological model proposed for TMEM16A. TMEM16 operates as a dimer according to initial biochemical analyses and to the structural studies [25].

Within this background, we report here the establishment of a microscopy-based traffic assay on the physiologically relevant CFBE (CF Bronchial Epithelial) cell line stably transduced to express a reporter of ANO1 traffic under an inducible promoter. This ANO1 traffic reporter contains enhanced green fluorescent protein (eGFP) fused to the C-tail of ANO1 and a triple hemagglutinin (3HA) tag at its first extracellular loop so as to detect PM localized ANO1 by use of anti-HA antibody without cell permeabilization. Similarly to previously described for CFTR [26], this double-tagged reporter allows for ratiometric readouts of traffic efficiency on a single cell basis, thus constituting a reliable cellular model to study ANO1 traffic. Results shown here for this cellular model demonstrate the robustness and sensitivity of the assay. Applying this assay in systematic loss-of-function (siRNA knock-down) gene screens [27] will allow identification of ANO1 traffic regulators and potential drug targets for CF.

2. Methods

2.1. ANO1 construct and cell line generation

A novel cell line derived from the CF Bronchial Epithelial (CFBE) cell line was generated to stably express a double-tagged ANO1 construct (Fig. 1a) with enhanced green fluorescent protein (eGFP) fused to its C-tail (via a small linker: LEFLNCCPGCCMEPSTT) and with a hemagglutinin tag (YPYDVPDYA) inserted in triplicate (3HA) between His³⁹⁶ and Asn³⁹⁷, i.e., in the first extracellular loop of ANO1 (Fig. S1). The numbering corresponds to ANO1 isoform X5 (NCBI Reference Sequence: XP_011543427.1). First the 3HA-ANO1-eGFP construct was cloned into the pLVX-TRE3G inducible lentiviral vector (Clontech, Enzifarma S.A., Portugal), using the In Fusion® HD Cloning Kit (Clontech). After confirmation of correct tags insertion by sequencing, the pLVX-TRE3G-3HA-ANO1-eGFP construct was transfected into HEK (Human Embryonic Kidney) 293 T cells to produce lentiviral particles which

were used to transduce parental CFBE cells. After culturing in selection media, cells were sorted by flow cytometry in a BC MoFlo Cell Sorter (Beckman Coulter, Inc., Indianapolis IN, USA) to select for high eGFP fluorescence (Fig. S2). The selected 3HA-ANO1-eGFP expressing cells indeed displayed not just enhanced but also more homogeneous levels of ANO1 (Fig. S3). The inducibility of ANO1 in this cell line was also confirmed by Western blot (WB) with the antibody DOG1 (Fig. 1b), demonstrating the higher levels of ANO1 in induced vs non-induced cells (with some leaky expression from the Tet-On promoter). Endogenous ANO1 protein is not detected since it is expressed at much lower levels.

2.2. Cell culture

3HA-ANO1-eGFP CFBE cells were cultured EMEM-Eagle's Minimum Essential Media with L-Glutamine (BE12-611F, Lonza – BioWhittaker, Switzerland) supplemented with 10% (v/v) heat inactivated fetal calf serum (Gibco #10106), 400 µg/ml G418 (Sigma-Aldrich, A1720) and 2 µg/ml puromycin (Invivogen #ant-pr-1) at 37 °C and 5% CO_2 . Uncoated 10 cm plastic Petri dishes were used (Nunc™ #150350).

2.3. Western blotting (WB)

For WB, 3HA-ANO1-eGFP CFBE cells were collected and lysed in 0.5% (v/v) NP40 lysis buffer. Proteins were separated by 7% (w/v) SDS-PAGE and transferred into PVDF membrane. Membrane was blocked with 5% (w/v) Non-fat milk powder (NFM) in Tris buffer saline with Tween 20 (TBS-T) for 1 h at room temperature and incubated overnight at 4 °C with rabbit DOG1 antibody (Novus Biologicals, # NP_060513) diluted 1:500 in 1% (w/v) NFM/TBS-T. The membrane was incubated with HRP-conjugated goat anti-rabbit IgG (diluted 1:10,000 in 1% NFM/TBS-T) for 2 h at room temperature. Subsequently, the immunoreactive signals were detected using a SuperSignal West Pico chemiluminescence substrate (Pierce).

2.4. Ussing chamber experiments

For open circuit measurements 3HA-ANO1-eGFP CFBE cells were seeded at approximately 3.5×10^5 cells/ml onto Costar Transwell® permeable supports of pore size 0.4 µm (Snapwell, Corning-Costar®, Tewksbury, MA, USA) and 1.13 cm² area. Transepithelial electrical resistance (TEER) of the 3HA-ANO1-eGFP CFBE monolayers was measured with a chopstick electrode (STX2 from WPI®, Berlin, Germany) and electrophysiological analyses were carried out in monolayers with resistance values above 600 Ω × cm². Transepithelial resistance R_{te} was determined by applying 1 s current pulses of 0.5 µA (5 s-period). For Ussing chamber measurements, Snapwells were mounted in the chamber device and continuously perfused with Ringer containing (mM): NaCl 145, K₂HPO₄ 1.6, MgCl₂ 1, KH₂PO₄ 0.4, Ca²⁺ Gluconate 1.3, Glucose 5, pH -7.4. ANO1 was activated by ATP (100 µM) added to the luminal as well as to the basal side and inhibited by the CaCCinh-A01 (30 µM) [28]. Values for the transepithelial voltage (V_{te}) were referenced to the luminal epithelial surface. Equivalent short-circuit current (I_{eq-sc}) were calculated according to Ohm's law from V_{te} and R_{te} ($I_{eq-sc} = V_{te}/R_{te}$), with appropriate correction for fluid resistance.

2.5. Assessment of ANO1 activity by patch-clamp

Cells grown on cover slips were mounted in a perfused bath at about 10 ml/min on the stage of an inverted microscope (IM35, Zeiss) and kept at 37 °C. The bath was perfused continuously with Ringer solution (mM): NaCl 145, KH₂PO₄ 0.4, K₂HPO₄ 1.6, D-glucose 5, MgCl₂ 1, Ca-gluconate 1.3, pH 7.4. Patch-clamp experiments were performed in the fast whole-cell configuration. Patch pipettes had an input resistance of 4–6 MΩ, when filled with an intracellular like solution containing (mM): KCl 30, K-gluconate 95, NaH₂PO₄ 1.2, Na₂HPO₄ 4.8, EGTA 1, Ca-

gluconate 0.209, MgCl₂ 2.38, D-glucose 5, ATP 3 (pH 7.2), the Ca²⁺ activity was 0.1 μM. The access conductance was measured continuously and was 90–140 nS (EPC 9 amplifier, List Medical Electronics, Darmstadt, Germany). In regular intervals, membrane voltages (Vc) were clamped in steps of 20 mV from –100 to +100 mV from holding potential of –60 mV.

2.6. Preparation of siRNA coated multi-well plates and ANO1 traffic assay

Multi-well plates (BD Falcon #353962) were coated with customized siRNAs for solid-phase reverse transfection adapted from a previously reported protocol [29] with adjustments also described before [26]. The siRNAs used here were (Silencer® Select, Ambion): siCOPB1 (#s3371); siESYT1 (#s23605, #s23606); siANO1 (#s30184) and the siScrb1 described before [30]. In addition #s23607 was used for immunofluorescence validation of all functional experiments.

3HA-ANO1-eGFP CFBE cells were grown to confluence and split (50%). Twenty-four hours later, cells were trypsinized to antibiotic-free medium and seeded in siRNA coated 384-well plates (50 μl/well, 3 × 10³ cells/well) using a Multidrop™ Combi peristaltic dispenser (Thermo Scientific #5840300). ANO1 expression was induced for 48 h (24 h after seeding) with antibiotic-free medium supplemented with 1 μg/ml doxycycline (Sigma #9891).

2.7. Liquid siRNA transfection

Liquid siRNA transfection of 3HA-ANO1-eGFP CFBE cells was carried out by Lipofectamine 3000 (Invitrogen) using siRNAs that target extended synaptotagmins 1, 2, 3 (siESYT1, siESYT2 and siESYT3) or coatomer subunit beta (siCOPB1). The expression of 3HA-ANO1-eGFP was induced by addition of 1 μg/ml doxycycline (Dox) 24 h after transfection. Experiments were performed 72 h after transfection (48 h of Dox induction). All siRNAs were obtained from Ambion® (Silencer® Select).

2.8. Immunostaining

Extracellular HA-tag was immunostained in non-permeabilized cells 72 h after seeding. After culture medium removal, cells were washed once with ice cold PBS and incubated 1 h at 4 °C with monoclonal anti-HA antibody (5 μg/ml, Biolegend # 901502).

Then, cells were washed 3 times with ice cold PBS, incubated 20 min with 3% (w/v) paraformaldehyde (PFA) at 4 °C and transferred to room temperature for the remaining staining procedure. Cells were then washed three times with PBS and incubated 1 h with an anti-mouse Alexa Fluor® 647 conjugated secondary antibody (2 μg/ml Molecular Probes #A31571). Cells were then washed 3 times with PBS and incubated with a Hoechst 33,342 solution (200 ng/ml, Sigma #B2261) for 1 h. Finally, cells were washed three times with PBS, immersed in PBS and incubated overnight before imaging.

All solutions were prepared in Dulbecco's PBS freshly supplemented with 0.7 mM CaCl₂ and 1.1 mM MgCl₂. Antibody solutions additionally contained 1% (w/v) bovine serum albumin (BSA, Sigma-Aldrich #A9056). All liquid handling was performed with a manual 96 channel pipette liquidator (Liquidator™ 96, Mettler Toledo #17010335). Solution volumes were (μl/well): 15 antibodies, 25 PFA, 50 Hoechst.

2.9. Image acquisition of fixed samples and time-lapse microscopy

Cell imaging for both fixed samples and time-lapse was performed with (automated) widefield epifluorescence microscope with a ScanR software (Olympus Biosystems) equipped with motorized stage and a metal halide light source (MT20), a 12-bit 1344 × 1024 pixel resolution C8484 CCD camera (Hamamatsu OrcaFlash4) and a 10 × or 20 × UPlanApo objectives (Olympus) and 0.4 or 0.7 of numerical aperture, for fixed samples and time-lapse imaging, respectively. Exposure times

for fixed samples at maximum light brightness were for Hoechst, eGFP and Alexa Fluor® 647 of (ms) 10–20, 500 and 2000, respectively. Time-lapse images were obtained each 30 min (for Dox induction) or 60 min (Dox removal), with exposure times of 150 ms (only eGFP). The Hoechst channel was used for contrast-based autofocus (fixed samples) and hardware auto focus for time-lapse imaging. Fixed samples were imaged at room temperature and live cells at 37 °C, 5%CO₂ in an environmental humidified microscope incubator. Filter settings (Excitation wavelengths/excitation band (nm) – Ex, Emission wavelengths/emission band (nm) – Em): Hoechst – Ex 347/50, Em 460/50; eGFP – Ex 470/40, Em 525/50; Alexa 647 – Ex 640/30, Em 690/50.

Fluorescence images in Fig. 1c were acquired with Leica TCS SP8 confocal microscope with a 60 × water objective with a numerical aperture of 1.4.

2.10. Analysis of time-lapse microscopy images

Time-lapse microscopy images were processed and quantified in Image J/Fiji. Briefly, a cell-free region was used for baseline correction. Then, representative cells were selected - i.e. cells which remain viable and within the field of view during the whole time-lapse - and their average fluorescence intensity was determined and plotted as a function of time. Finally, the grayscale lookup table was adjusted for optimal contrast.

2.11. Automatic image analysis pipeline

Automatic image analysis was performed with open source software tools (CellProfiler, R), using pipelines tailored to the specific application as described before for CFTR [26]. Initially, overall transfection efficiency was assessed by observing if cells transfected with siRNAs compromising chromosome segregation exhibited mitotic phenotypes [31]. Failure to observe these phenotypes in more than 75% of images implied the rejection of the corresponding plate from analysis. The algorithm for background subtraction was also described before [26]. Briefly, it comprised: 1) the computation of illumination correction functions for each fluorescence channel, which define the pixel-by-pixel fluorescence baseline for each channel as produced by image illumination and background fluorescence; 2) subtraction of the corresponding illumination correction function from each image. The pipeline includes quality control (QC) steps excluding cells which do not significantly express ANO1, have abnormal morphology (e.g. apoptotic cells) or contain a significant amount of saturated pixels. This fluorescence quantification data allowed determining ANO1 traffic in each cell according to the following formula:

$$\text{ANO1 Traffic Efficiency} = \frac{PM \text{ ANO1}}{\text{Total ANO1}} = \frac{\text{Alexa Fluor}^{\circledR} 647 \text{ Integrated Fluorescence}}{\text{GFP Integrated Fluorescence}} \quad (\text{Formula 1})$$

For each image, the ANO1 Traffic Efficiency was considered to be the median for all cells in the image, as previously described [26]. After averaging the ANO1 Traffic Efficiency for all images relating to the same siRNA, the effect of each siRNAs was compared with the one measured under the effect “Scrb1” non-targeting siRNA treatment ($\text{Traffic Efficiency}_{Neg.control}$) using the following formula:

$$\text{Deviation Score} = \frac{\text{Traffic Efficiency}_{Test} - \text{Traffic Efficiency}_{Neg.control}}{2 \times SEM_{Neg.control}} \quad (\text{Formula 2})$$

Where $SEM_{Neg.control}$ is the standard error of the mean for the Traffic Efficiency recorded upon “Scrb1” siRNA. We consider significant ANO1 Traffic Efficiency effects those whose magnitude is larger than twice the negative control. Thus, an ANO1 traffic enhancer has a Deviation Score

above + 1 and an ANO1 traffic inhibitor a Deviation Score below – 1. Additionally, two tailed Student's *t*-tests were performed to quantify statistical significance versus the corresponding negative control.

3. Results

Although ANO1 was previously reported to localize in the apical membrane of airway epithelial cells [17,20], we also first aimed to confirm this observation. Interestingly, specific staining of ANO1 in cryosections of human airways (CF and non-CF) evidenced that some ANO1 localizes to the apical surface, but there is a significant fraction which remains intracellularly located, particularly in CF airways (Fig. S4). These data thus emphasize the need to identify traffic regulators that promote ANO1 PM expression, so as to use this Cl[–] channel as a robust alternative to compensate for the absence of CFTR-mediated Cl[–] transport in CF.

3.1. ANO1 traffic reporter

The inducibility of the expression of 3HA-ANO1-eGFP traffic reporter (Figs. 1a, S1) by 1 µg/ml doxycycline (Dox) was confirmed by WB with the ANO1-specific antibody (anti-DOG1) showing a very significant increase in the levels of ANO1 in induced vs non-induced cells (Fig. 1b). We then determined the time course of the induction which starts to be noticeable after 6 h of Dox induction (Video S1, Fig. S5). PM localization of 3HA-ANO1-eGFP is observed after 13 h of Dox, becoming quite distinct from 20 h onwards (Video S1). Next, we assessed the stability of ANO1 expression after shutdown of transcription and our data indicate no reduction of ANO1 steady-state levels at least up to 13 h after Dox removal (Video S2).

Given its localization at an extracellular loop (Fig. 1a), the 3HA-tag only becomes exposed to the extracellular environment when the construct is inserted in the PM. Thus, its detection via immunofluorescence with anti-HA Ab-Alexa Fluor® 647 without cell permeabilization confirms the presence of 3HA-ANO1-eGFP at the cell surface (Fig. 1c). PM subcellular localization of the 3HA-ANO1-eGFP construct in CFBE cells is further supported by the orthogonal projection (z-plane) of a representative cell (Fig. 1d) showing that the anti-HA antibody staining is only observed at the PM. The 3HA-ANO1-eGFP CFBE cells were subject to cell sorting (see Methods) to optimize the homogeneous expression of the construct (Figs. S2, S3). The efficiency of ANO1 traffic can then be determined in individual cells using a ratiometric (Alexa Fluor® 647/eGFP) fluorescence microscopy-based measurement (see below).

3.2. Electrophysiological characterization

To functionally characterize the 3HA-ANO1-eGFP construct, Ussing chamber experiments in polarized cell monolayers of CFBE cells demonstrated that cells treated with Dox to induce 3HA-ANO1-eGFP expression exhibit equivalent short-circuit currents ($I_{eq-SC-ATP}$) upon stimulation with ATP (Fig. 2a, upper panels) which were significantly larger than those measured in non-induced cells (Fig. 2b). In order to determine that the observed differences were due to CaCC currents (and not to e.g., Ca²⁺-activated potassium (K⁺) channels), similar experiments were also performed in the presence of CaCC inhibitor A01 (Fig. 2a, lower panels), which showed a large decrease in ATP-induced currents, being the remaining observed currents no different between induced and in non-induced CFBE cells (Fig. 2b).

To further validate the physiological relevance of this cellular model as a bona fide platform for a screening platform, we next characterized the activity of the double-tagged ANO1 construct for their ability to conduct Cl[–] using the patch-clamp technique (Fig. 2c). Analysis of the whole-cell currents detected in Dox-treated cells upon ATP stimulation showed that, similarly to Ussing chamber data, were significantly larger than those measured in non-induced cells (Fig. 2d). Moreover, patch-clamp experiments were also performed in HEK 293 – as ANO1-null

cells – by transient transfection with the 3HA-ANO1-eGFP construct either with or without induction (Fig. S6). Doxycycline induced cells showed significantly increased current densities when compared with non-induced cells. PM expression of the double-tagged ANO1 construct was also confirmed in these cells (Fig. S7). Altogether, these data fully demonstrate that the double-tagged construct preserves the ANO1 functional integrity and thus likely its regulation by multiple protein interactions is preserved in the physiologically relevant CFBE cells.

3.3. siRNA microscopy-based traffic assay

To assess the suitability of the microscopy-based traffic assay as a platform to identify putative novel regulators of ANO1 traffic, we next performed reverse transfection in siRNA pre-coated microscopy plates. As previously optimized [26,32], a treatment time of 72 h for siRNAs was selected. Expression of the 3HA-ANO1-eGFP construct was induced during the last 48 h of siRNA treatment. Image quantification was performed with CellProfiler using the previously described analysis pipelines for CFTR: one to calculate the illumination correction (for background subtraction) and another to perform background subtraction, cell segmentation, fluorescence integration and basic quality control [26].

Screening a pilot siRNA library with the 3HA-ANO1-eGFP cell line revealed several siRNAs significantly affecting its traffic, as shown in representative immunofluorescence images (Fig. 3a). After expression induction of 3HA-ANO1-eGFP, a significant amount of ANO1 is detected at the PM in the negative control assay, i.e., “Scrambled” siRNA (siScrb1) treated cells. The high sensitivity and large dynamic range of this assay are shown by the significant changes in the fluorescence ratio of PM versus total ANO1 (Fig. 3b), for which the screen avgScores ranged between – 5.8 and + 5.4 (data not shown). In our pilot screen, we identified COPB1 siRNA (Fig. 3a, 2nd row from top) as a significant ANO1 traffic enhancer (avgScore = + 3.81), without increasing total ANO1 protein expression levels (Fig. S8) and the siRNA targeting ESYT1 - extended synaptotagmin-1 (Fig. 3a, 3rd row from top) gene as a reproducible traffic inhibitor (avgScore = – 1.67). Treatment with ANO1-siRNA (siANO1) significantly decreased the fluorescence signal in almost all cells (Fig. 3a, bottom row), indicating a high transfection efficiency as well as correct association of the Alexa Fluor® 647-fluorescence signal to ANO1-eGFP expression. Although the expression level is not totally homogenous across all cells, traffic efficiency is robust to such variations due to the ratiometric measurements.

3.4. Biological relevance of a hit: the role of extended synaptotagmin (ESYT1) on ANO1

In order to demonstrate the biological relevance and significance of this novel microscopy-based traffic assay, we showed the impact of extended synaptotagmin-1 (ESYT1) on ANO1 traffic and function. The reason why we chose ESYT1 (FAM62A) is because, besides having an interesting biological function (being an ER-PM tethering protein), this protein was also described as an ANO1 interactor in a previous proteomics study by Hartzell and colleagues [33]. Although ESYT2 and ESYT3 were not hits in such study, we decided to also assess their effect on ANO1, given their proximity to ESYT1. To this end, we performed additional experiments to determine both PM localization (immunostaining) after liquid transfection (see Methods) and function (patch-clamp) in 3HA-ANO1-eGFP CFBE cells transfected for 72 h with siRNAs targeting COPB1 as well as ESYT1, ESYT2 and ESYT3. Our immunostaining data (Fig. 4) demonstrate that the knockdown of COPB1 significantly increased ANO1 PM expression. Also by immunostaining, we observe that the knockdown of ESYT1 and ESYT2 significantly decreased ANO1 PM expression (Fig. 4); ESYT3 knockdown did not cause a significant change in ANO1 PM levels, but this is likely due to its very low levels in CFBE cells (Fig. S9).

Patch-clamp data (Fig. 5) demonstrate that COPB1 knockdown (KD)

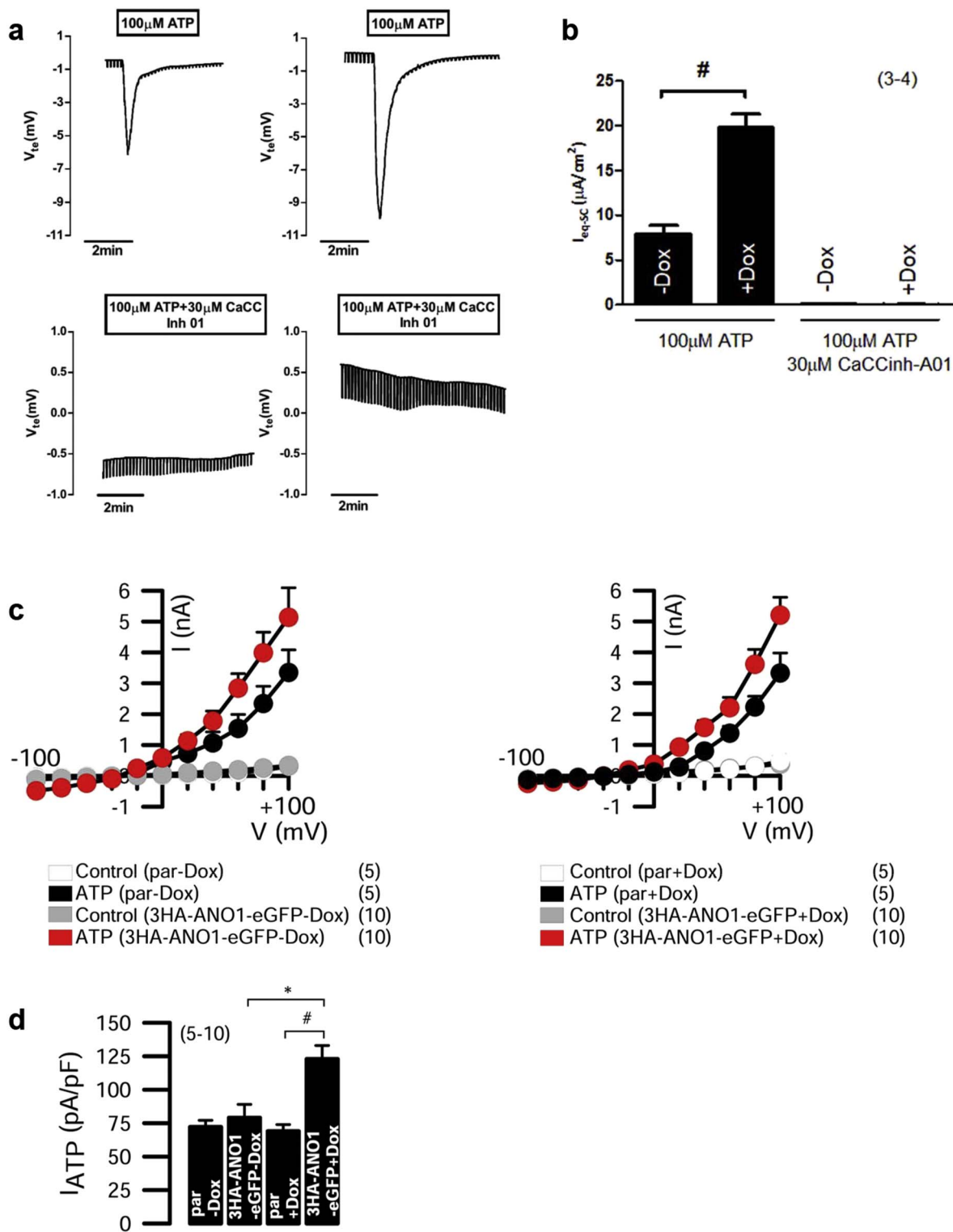


Fig. 2. Functional assessment of 3HA-ANO1-eGFP construct in CFBE cells by transepithelial Cl^- transport measurements in Ussing chamber and whole-cell patch-clamp. (a) Original Ussing chamber tracings obtained for ATP-induced Cl^- currents in the absence (top tracings) or in the presence (lower tracings) of CaCC inhibitor AO1 for 3HA-ANO1-eGFP CFBE cells non-induced (left) or after Dox induction (right); (b) Summary of I_{sc-eq} currents of 3HA-ANO1-eGFP CFBE cells non-induced (- Dox) or after Dox induction (+ Dox). Data are represented by mean \pm SEM and statistical analyses were performed by GraphPad Prism 5.0 using unpaired *t*-test where “#” indicates statistical significant difference ($p \leq 0.05$). Functional assessment of 3HA-ANO1-eGFP construct in CFBE cells vs parental CFBE cells by whole-cell patch-clamp; (c) Current/voltage (*I/V*) curves -100 mV to +100 mV for 3HA-ANO1-eGFP (grey, red) and parental (white, black). CFBE cells in Ringer (white, grey) or after stimulation with 100 μ M ATP (black, red) non-induced (left) or after Dox induction (right). All solutions contained 50 nM TRAM 34, a potassium (K^+) channel inhibitor to discard K^+ currents and the number (n) of experiments is indicated in front of each label. (d) Delta of the average of ATP-induced current densities. “*” indicates statistical significance of induced (+ Dox) vs non-induced (- Dox) 3HA-ANO1-eGFP CFBE cells ($p \leq 0.05$ in unpaired *t*-test) and “#” indicates statistical significance of 3HA-ANO1-eGFP vs parental CFBE cells ($p \leq 0.05$ in unpaired *t*-test).

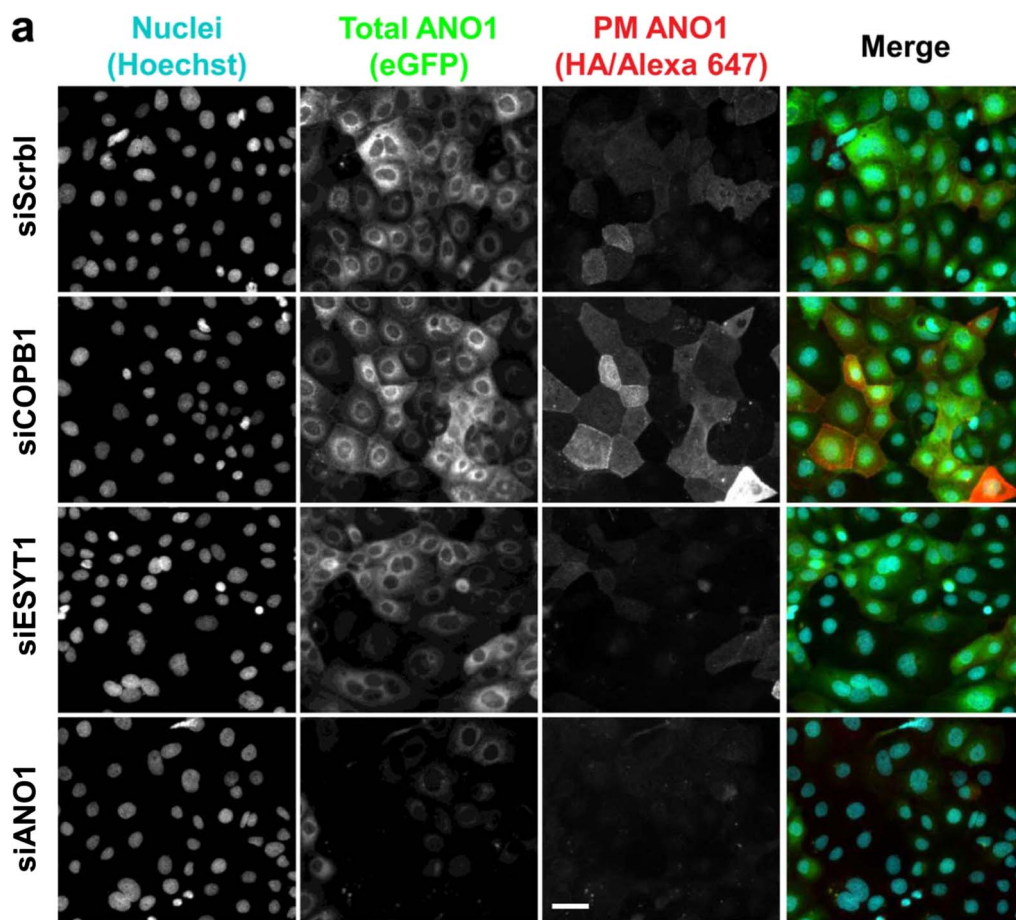
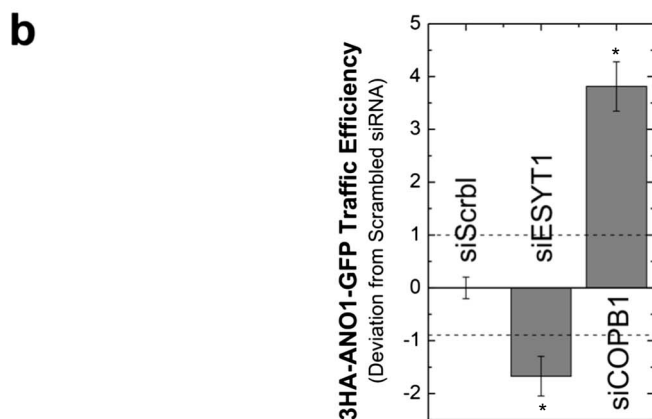


Fig. 3. Representative widefield epifluorescence microscopy images obtained for the ANO1 traffic screen. (a) CFBE cells expressing the 3HA-ANO1-eGFP construct were treated with distinct siRNAs and stained with the anti-HA antibody without cell permeabilization (see [Methods](#)). Treatment with a siRNA targeting ANO1 itself (siANO1) shows a specific detection of ANO1 and a high transfection efficiency (Bottom row). Knocking down COPB1 (siCOPB1) significantly enhanced traffic of 3HA-ANO1-eGFP (2nd row from top) and knocking down ESYT1 (siESYT1) significantly decreased it (2nd row from bottom). Images were acquired in an Olympus Scan'R microscope. Exposure times at maximum light brightness for Hoechst, eGFP and Alexa Fluor® 647 were 10–20 ms, 500 ms and 2000 ms, respectively. Scale bar = 50 μ m. Images were quantified to determine traffic efficiency ([Formula 1](#), see [Methods](#)). (b) Data are presented as the mean deviation to negative controls \pm SD for all siRNAs with the mentioned targets and ‘*’ represents statistical significance of COPBP or ESYT1 vs Scrambled siRNA ($p \leq 0.01$) in a Welch Two-Sample *t*-test.



significantly increases ANO1 current density, compared to scrambled siRNA transfected cells, used as negative control ([Fig. 5b](#)) and that knockdown of ESYT1, ESYT2 and ESYT3 significantly decrease ANO1 current density, also in comparison to scrambled siRNA transfected cells ([Fig. 5b](#)).

Our approach to address the specificity of the siRNA ESYT1 experiments was 2-fold: 1) by targeting ESYT1 with three different siRNAs, namely (see [Methods](#)): s23605 and s23606 (both used in the screen with negative scores of -1.4 and -1.9, respectively) and s23607 which was used in immunofluorescence validation as well as in all functional experiments; 2) by showing the correspondent decrease on ESYT1 mRNA levels ([Fig. S9](#)).

Further, to determine the specificity of COPB1 and ESYT1 on ANO1,

we tested their effects on another PM protein – the epidermal growth factor receptor (EGFR) by cell-surface biotinylation. Our data ([Fig. S10](#)) show that the knockdown of either siCOPB1 or siESYT1 does not alter PM levels of EGFR.

Moreover, we performed additional experiments to determine whether the regulatory mechanisms determined here for 3HA-ANO1-eGFP also apply to endogenously expressed ANO1 in parental CFBE cells ([Fig. S11](#)). These data indeed demonstrate that the impact of screen hits COPB1 and ESYT1 on endogenous ANO1 function is similar to that observed for 3HA-ANO1-eGFP (compare with data in [Fig. 5](#)) being thus physiologically relevant.

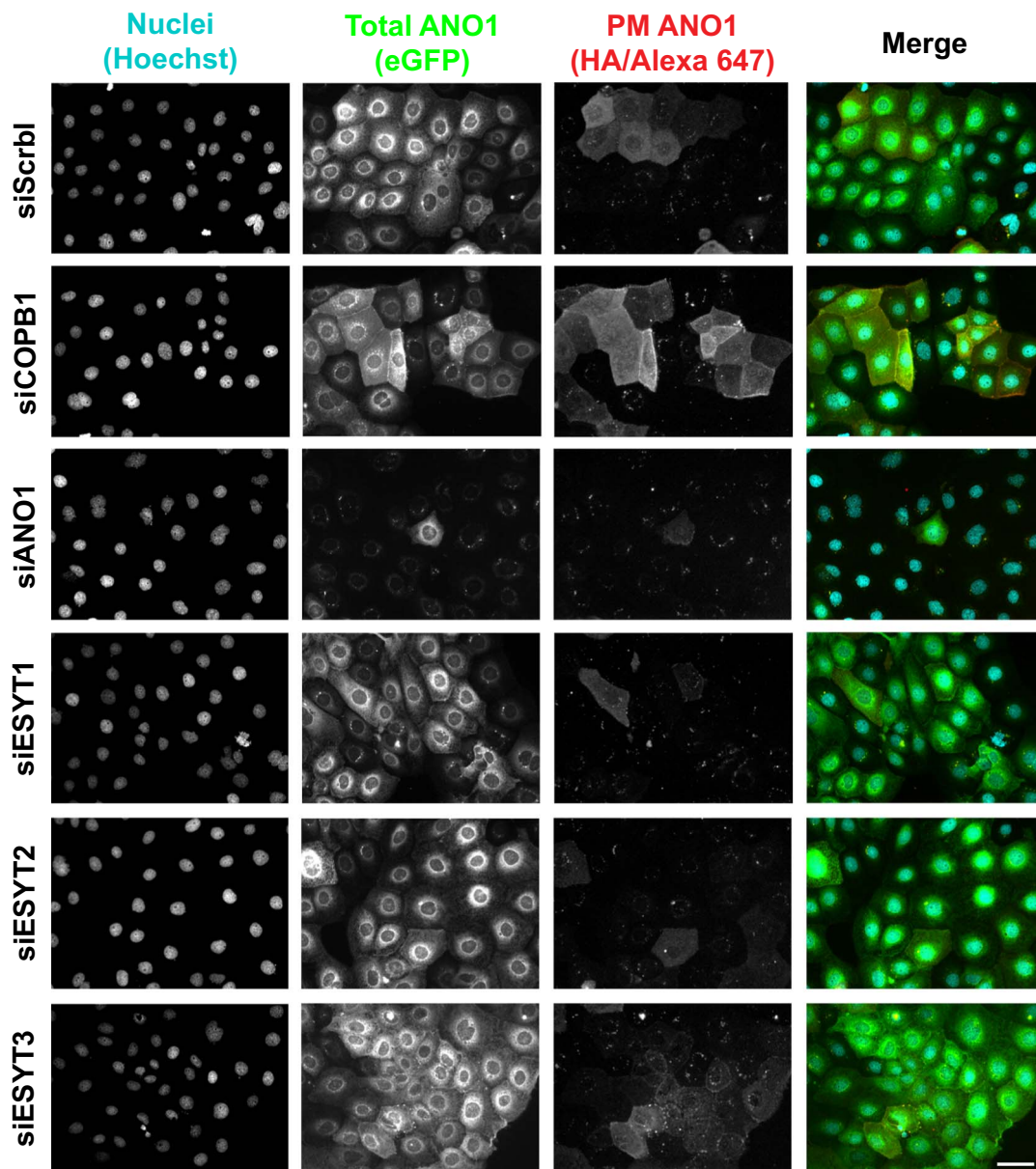


Fig. 4. Confirmation of effects of screen hits on ANO1 PM localization. Representative widefield epifluorescence microscopy images were obtained after liquid siRNA transfection of 3HA-ANO1-eGFP CFBE cells with distinct siRNAs (see [Methods](#)) and stained with the anti-HA antibody without cell permeabilization as in [Fig. 3](#). Treatment with an siRNA targeting ANO1 (siANO1) shows once more a specific detection of ANO1 and a high transfection efficiency. Traffic of 3HA-ANO1-eGFP was greatly enhanced by knocking-down COPB1 (siCOPB1) and significantly decreased by knocking-down ESYT1 (siESYT1) and ESYT2 (siESYT2). The knock-down of ESYT3 (siESYT3) did not seem to cause any effect on ANO1 PM levels, what must be due to its very low expression levels in CFBE cells (see [Fig. S9](#)). Images were acquired with an Axiovert 200 M fluorescence microscope (Zeiss, Jena, Germany), using a 20 × dry objective. Scale bar = 50 μm.

4. Discussion

4.1. Overall features of the cell-based ANO1 traffic assay

Herein we report the development of a new cell-based assay for the identification of regulators of ANO1. Indeed, scaling-up of the current assay to high-throughput screening (HTS) microscopy allows to identify on a global scale genes regulating ANO1 traffic and also drug discovery. So far, no traffic studies have been conducted for this clinically relevant protein mostly because no good cellular model was available. Yet, this is a crucial aspect to our mechanistic understanding of ANO1 physiological and pathological role.

The new tool described here includes a novel cell line expressing an inducible ANO1 traffic reporter, a traffic assay adequate to be scaled-up for microscopy-based HTS and an automated quantification method.

We have validated this traffic assay by applying it to a small number of siRNAs. These siRNA experiments showed that the ANO1 traffic assay is specific (as evidenced by control siRNAs) and robust (good dynamic range), thus demonstrating that it can be used to identify gene regulators of ANO1 traffic as potential drug targets.

As already previously described for a similar screening platform [26], the current tool has various major advantages vs other alternative assays, such as the one measuring ANO1 activity in FRT cells [34–36]. These advantages include: *i*) the conditional (Tet-inducible) expression of ANO1 which allows assessing the effects of genes/compounds before the target protein (ANO1) is expressed, so as to detect their impact on the early stages of secretory traffic; *ii*) the double-tagged construct allows for a ratiometric readout (the protein fraction at the PM vs total protein expressed); and *iii*) the microscopy approach employed for the current assay enables the application of a quality control based on

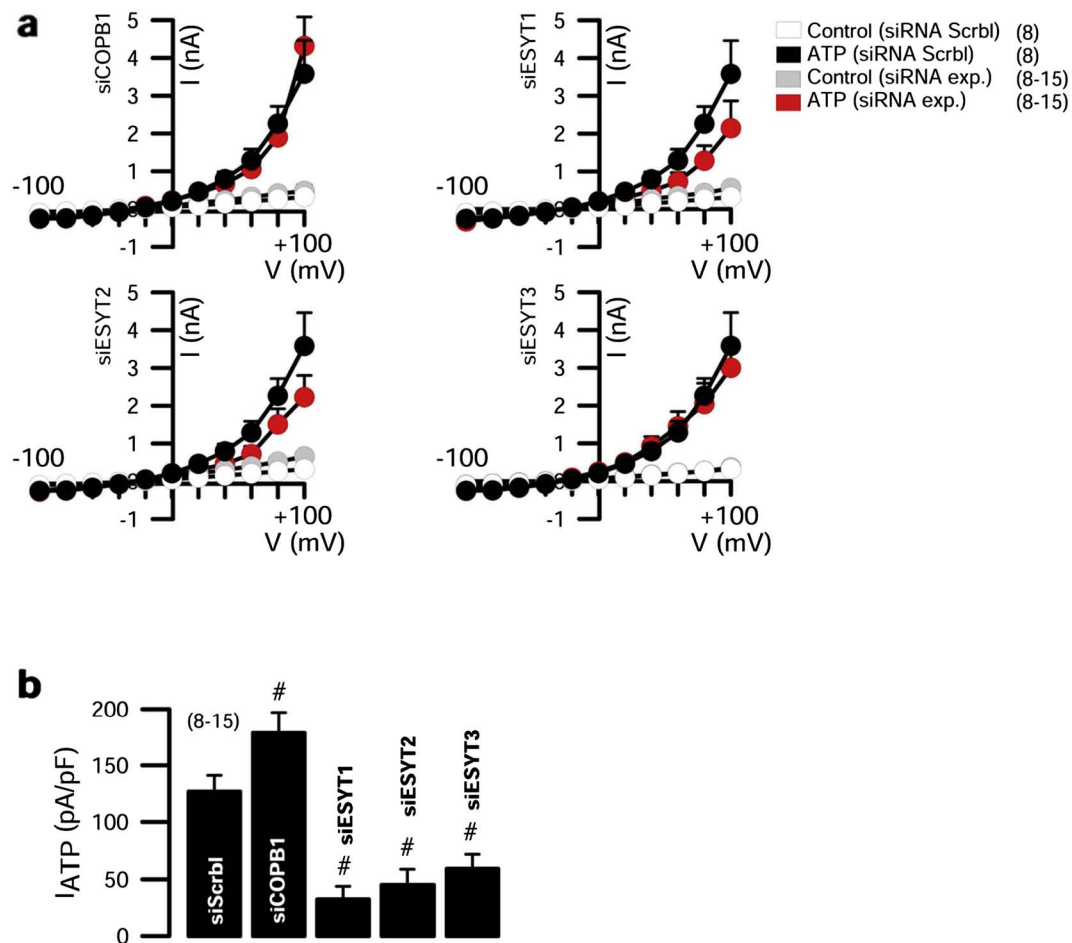


Fig. 5. Impact of screen hits on ANO1 function. (a) Whole-cell patch-clamp data obtained for 3HA-ANO1-eGFP CFBE cells induced with doxycycline and transfected with siRNAs targeting COPB1 (upper left), ESYT1 (upper right), ESYT2 (lower left), ESYT3 (lower right) or scrambled (control). Current/voltage (I/V) curves -100 mV to +100 mV for each siRNA under test (grey, red) or Scrambled (white, black) in Ringer (white, grey) or after stimulation by 100 μ M ATP (black, red). All solutions contained 50 nM TRAM 34, a potassium (K^+) channel inhibitor to discard K^+ currents and the number (n) of experiments is indicated in front of each label. (b) Delta of the average of ATP-induced current densities. ‘#’ indicates statistical significance of ATP-stimulated currents of the respective siRNA vs Scrambled ($p \leq 0.05$ in unpaired *t*-test).

several cell parameters (e.g., total number of cells, cell shape, cell size, etc) and statistical analyses based on individual cells, which is not possible in the plate reader. Such characteristics make the current assay to be of higher potential for screening to the previously reported methods.

4.2. A tool to study physiological regulation of ANO1

The current novel cellular model clearly demonstrates that ANO1 localizes to the PM, recapitulating the initially reported findings [17,20]. This constitutes a crucial requirement for the physiological relevance of this assay in CF biomedical research. In some neuron subtypes the ANO1 PM localization was described to be restricted to just specific membrane domains [21] and the fungal homologue nhTMEM16 was not found to be present at all at them PM when heterologously expressed in HEK cells [23]. Although ANO1 was reported to localize in the apical membrane of airway epithelial cells [17,20], our data show that ANO1 occurs mostly at the apical surface of non-CF bronchial epithelia, but it remains largely intracellularly localized in CF epithelia.

Admittedly, our assay employed a double-tagged construct and the cellular sorting of CFBE cells for high expression levels, which are far from physiological context. Nevertheless, our data demonstrate that the impact of screen hits COPB1 and ESYT1 on endogenous ANO1 function is similar to that observed for 3HA-ANO1-eGFP. Therefore, and as demonstrated for our siRNA data shown here, the use of this cellular

model can help identify physiologically relevant genes and/or compounds that regulate ANO1 PM traffic, having thus potential to be used in functional genomic screens.

Indeed, in the siRNA experiments performed here, we identified that siCOPB1, a component of the COPI trafficking machinery enhances the PM localization of ANO1. Although COPI has been implicated in secretory traffic between the Golgi and the ER both in the anterograde and retrograde direction, inhibition of one COPI component with enhanced ANO1 at PM is in line with the observed increase in the anterograde traffic of some PM proteins, such as CFTR [26]. Moreover, and confirming the present data, a recent study [37] also described that ANO1 cell surface expression of is suppressed by protein-protein interactions with β -COP, of which COPB1 is a component.

We also found that siESYT1 inhibits ANO1 PM traffic, thus indicating that the extended synaptotagmin-1 protein should promote the PM insertion of ANO1.

4.3. Physiological relevance of ESYT1 in promoting PM traffic of ANO1

Interestingly, ESYT1 is a member of the extended synaptotagmins (ESYTs) family of proteins with a new role in tethering the ER to the PM in a Phosphatidylinositol 4,5-bisphosphate (PIP₂) - and Ca²⁺- dependent way [38]. This is consistent with the localization of ANO1 yeast analogue Ist2 at these ER-PM junctions [39] and the recently proposed role of anoctamins in generating compartmentalized Ca²⁺ signals [23]. Interestingly, ESYTs participate in lipid transfer between the ER and PM

[40], a role somewhat related to the scramblase function of some anoctamins. Thus, we have chosen ESYT1 and the two other members of this protein family – ESYT2 and ESYT3 – to be examined in more detail using immunostaining and patch-clamp analysis. The three ESYTs are ER proteins that participate in such tethering function via C2 domain-dependent interactions with the PM that require PIP₂ in the case of ESYT2 and ESYT3 and also elevation of cytosolic Ca²⁺ in the case of ESYT1 [38]. Although ESYT-dependent contacts are not required for store-operated Ca²⁺ entry, we found a clear inhibitory effect on receptor-mediated activation of ANO1 which was confirmed by decreased PM levels of ANO1. This is somewhat surprising as the ESYTs are shown not to participate in the targeting of InsP₃Rs to the apical region of hepatocytes [41]. Thus, although it was shown that the simultaneous loss of all three ESYTs has no effect on overall development and survival of mice, genes encoding Orp5/8, Ora1, STIM1 and TMEM110, other ER-PM membrane junction proteins are upregulated, which could potentially compensate for ESYT loss [42,43]. Our observation that GPCR-mediated activation of ANO1 is compromised in cells with knockdown of ESYTs suggests that the Ca²⁺ dependent lipid transfer between ER membrane and PM is compromised, which also fits to the earlier observation of an enhanced and sustained accumulation of PM diacylglycerol (DAG) following PIP₂ hydrolysis by PLC activation [44].

4.4. Potential of the ANO1 traffic assay for disease-related studies

In the context of CF, the ANO1 traffic assay described here allows for: (i) identification of regulators of ANO1 traffic (potential drug targets); (ii) development of compounds modulating high-potential drug targets from (i); (iii) direct discovery of compounds modulating ANO1 traffic; (iv) gaining insight into mechanisms of ANO1 secretory traffic. Moreover, insertion of the current construct into the previously described CFBE models of normal and mutant double-tagged CFTR [26] will also provide mechanistic insight into one currently ANO1 key question, i.e., whether and how are the traffic of ANO1 and CFTR co-regulated.

Besides its relevance for CF, ANO1 has also been reported to be a major player in tumorigenesis, having high ANO1 expression levels been reported in multiple forms of cancer (reviewed in [23]). Although it is still unclear whether such high levels are cause or consequence of carcinogenesis, the current platform also allows for the identification of negative regulators of ANO1 traffic as exemplified here for ESYT1. This demonstrates that the current assay enables similar workflows to identify traffic enhancers and inhibitors alike. Also, the 3HA-ANO1-eGFP construct could also be used to transform cellular models which could be more relevant to these pathologies.

ANO1 was likewise proposed to modulate mucin secretion and airway muscle contraction [45] contributing to airway hyperresponsiveness [46,47]. These studies suggest that it may constitute a therapeutic target for limiting airway constriction in asthma, in which case it would be important to look for ANO1 inhibitors. Although more recently ANO1 was also described to have a protective role in the hyperresponsiveness of airway cells to lipopolysaccharide (LPS) [48], the current traffic assay can be of equal value to identify inhibitors/enhancers as well as to help clarifying a mechanistic role for ANO1 also in these processes.

Anoctamins have been described to operate as dimers, as also confirmed by high-resolution structural analysis of the fungal homologue nhTMEM16 [24]. Nonetheless very little is known regarding the formation of heterodimers as well as on the properties of different ANO dimers combinations. Insertion of similarly tagged constructs of other anoctamins into the current CFBE cell model will certainly be useful to gain functional and mechanistic insight into such heterodimer combinations of ANO1.

Altogether, many studies on ANO1 report a broad range of yet poorly understood properties many of high relevance to multiple diseases. The cellular model and traffic assay reported here can help shed

light into these biological processes by the global identification of the intervenients in the molecular and cellular pathways underlying these conditions.

In conclusion, the ANO1 traffic assay reported here is an improvement over current strategies for ANO1-based drug development for several human diseases, namely for CF. Moreover, it can also be used in functional genomic (siRNA/cDNA) screens to identify genes which regulate ANO1 traffic which may be used as pharmacological targets to bypass the lack of functional CFTR in CF patients.

This work model will also set the stage for a better knowledge of ANO1 traffic, regulation and its relation with CFTR.

Supplementary data to this article can be found online at <https://doi.org/10.1016/j.bbamcr.2017.11.009>.

Author contributions

RP, KK and MDA designed the research. JRL, MCP, HMB, NTA, MCQ, IALS, PW and RS performed experiments. JRL, MCP, HMB, NTA, IALS and RS analyzed data. JRL, MCP, HMB and MDA wrote the manuscript RP and KK revised the manuscript.

Competing financial interests

The authors declare no competing financial interests.

Transparency document

The Transparency document associated with this article can be found, in online version.

Acknowledgements

Work supported by UID/MULTI/04046/2013 centre grant from FCT, Portugal (to BioISI) and CF Trust Strategic Research Centre Award (Ref. SRC 003) “INOVCF” (to MDA, KK and RP); A12 DFG-SFB699 A7/A12 and DFG KU756/12-1 projects (both to KK). JRL, MCP, NTA and MCQ are recipients of fellowships from BioSys PhD programme (Refs SFRH/BD52489/2014, SFRH/PD/BD/114393/2016, SFRH/BD/94486/2013, and SFRH/PD/BD/114389/2016, respectively) and HMB of a post-doctoral fellowship (SFRH/BPD/93017/2013) all from FCT (Portugal). The authors are also grateful to Luís Marques (BioISI) and to staff from EMBL, Heidelberg (Germany), namely from ALMF-Advanced Light Microscopy (Beate Neumann, Christian Tischer, Sabine Reither) and Flow Cytometry (Malte Paulsen and Diana Ordonez) core facilities for technical assistance.

References

- [1] S.C. Bell, K. De Boeck, M.D. Amaral, New pharmacological approaches for cystic fibrosis: promises, progress, pitfalls, *Pharmacol. Ther.* 145 (2015) 19–34, <http://dx.doi.org/10.1016/j.pharmthera.2014.06.005>.
- [2] K. De Boeck, M.D. Amaral, Progress in therapies for cystic fibrosis, *Lancet Respir. Med.* 2600 (2016) 1–13, [http://dx.doi.org/10.1016/S2213-2600\(16\)00023-0](http://dx.doi.org/10.1016/S2213-2600(16)00023-0).
- [3] M.D. Amaral, K. Kunzelmann, Molecular targeting of CFTR as a therapeutic approach to cystic fibrosis, *Trends Pharmacol. Sci.* 28 (2007) 334–341, <http://dx.doi.org/10.1016/j.tips.2007.05.004>.
- [4] Y.D. Yang, H. Cho, J.Y. Koo, M.H. Tak, Y. Cho, W.-S. Shim, S.P. Park, J. Lee, B. Lee, B.-M. Kim, R. Raouf, Y.K. Shin, U. Oh, TMEM16A confers receptor-activated calcium-dependent chloride conductance, *Nature* 455 (2008) 1210–1215, <http://dx.doi.org/10.1038/nature07313>.
- [5] A. Caputo, E. Caci, L. Ferrera, N. Pedemonte, C. Barsanti, E. Sondo, U. Pfeiffer, R. Ravazzolo, O. Zegarra-Moran, L.J. Galletta, TMEM16A, a membrane protein associated with calcium-dependent chloride channel activity, *Science* 322 (2008) 590–594, <http://dx.doi.org/10.1126/science.1163518>.
- [6] B.C. Schroeder, T. Cheng, Y.N. Jan, L.Y. Jan, Expression cloning of TMEM16A as a calcium-activated Chloride Channel subunit, *Cell* 134 (2008) 1019–1029, <http://dx.doi.org/10.1016/j.cell.2008.09.003>.
- [7] A.B. Stephan, E.Y. Shum, S. Hirsh, K.D. Cygnar, J. Reiser, H. Zhao, ANO2 is the ciliary calcium-activated chloride channel that may mediate olfactory amplification, *Proc. Natl. Acad. Sci. U. S. A.* 106 (2009) 11776–11781, <http://dx.doi.org/10.1073/pnas.0903304106>.

- [8] J.R. Martins, D. Faria, P. Kongsuphol, B. Reisch, R. Schreiber, K. Kunzelmann, Anoctamin 6 is an essential component of the outwardly rectifying chloride channel, *Proc. Natl. Acad. Sci.* 108 (2011) 18168–18172, <http://dx.doi.org/10.1073/pnas.1108094108>.
- [9] K. Kunzelmann, Y. Tian, J.R. Martins, D. Faria, P. Kongsuphol, J. Ousingsawat, F. Thevenod, E. Roussa, J. Rock, R. Schreiber, Anoctamins, *Pflugers Arch. - Eur. J. Physiol.* 462 (2011) 195–208, <http://dx.doi.org/10.1007/s00424-011-0975-9>.
- [10] N. Pedemonte, L.J.V. Galiotta, Structure and function of TMEM16 proteins (anoctamins), *Physiol. Rev.* 94 (2014) 419–459, <http://dx.doi.org/10.1152/physrev.00039.2011>.
- [11] J. Suzuki, T. Fujii, T. Imao, K. Ishihara, H. Kuba, S. Nagata, Calcium-dependent phospholipid scramblase activity of TMEM16 protein family members, *J. Biol. Chem.* 288 (2013) 13305–13316, <http://dx.doi.org/10.1074/jbc.M113.457937>.
- [12] J.M. Whitlock, H.C. Hartzell, Anoctamins/TMEM16 proteins: chloride channels flirting with lipids and extracellular vesicles, *Annu. Rev. Physiol.* 79 (2017) 119–143, <http://dx.doi.org/10.1146/annurev-physiol-022516-034031>.
- [13] A. Picollo, M. Malvezzi, A. Accardi, TMEM16 proteins: unknown structure and confusing functions, *J. Mol. Biol.* 427 (2015) 94–105, <http://dx.doi.org/10.1016/j.jmb.2014.09.028>.
- [14] J. Ousingsawat, J.R. Martins, R. Schreiber, J.R. Rock, B.D. Harfe, K. Kunzelmann, Loss of TMEM16A causes a defect in epithelial Ca²⁺ - dependent chloride transport, *J. Biol. Chem.* 284 (2009) 28698–28703, <http://dx.doi.org/10.1074/jbc.M109.012120>.
- [15] J.R. Rock, W.K. O'Neal, S.E. Gabriel, S.H. Randell, B.D. Harfe, R.C. Boucher, B.R. Grubb, Transmembrane protein 16A (TMEM16A) is a Ca²⁺ - regulated Cl⁻ secretory channel in mouse airways, *J. Biol. Chem.* 284 (2009) 14875–14880, <http://dx.doi.org/10.1074/jbc.C109.000869>.
- [16] V.G. Romanenko, M.A. Catalán, D.A. Brown, I. Putzier, H.C. Hartzell, A.D. Marmorstein, M. Gonzalez-Begne, J.R. Rock, B.D. Harfe, J.E. Melvin, Tmem16A encodes the Ca²⁺ - activated Cl⁻ channel in mouse submandibular salivary gland acinar cells, *J. Biol. Chem.* 285 (2010) 12990–13001, <http://dx.doi.org/10.1074/jbc.M109.068544>.
- [17] P. Scudieri, E. Caci, S. Bruno, L. Ferrera, M. Schiavon, E. Sondo, V. Tomati, A. Gianotti, O. Zegarra-Moran, N. Pedemonte, F. Rea, R. Ravazzolo, L.J.V. Galiotta, Association of TMEM16A chloride channel overexpression with airway goblet cell metaplasia, *J. Physiol.* 590 (2012) 6141–6155, <http://dx.doi.org/10.1113/jphysiol.2012.240838>.
- [18] J. Jung, J.H. Nam, H.W. Park, U. Oh, J.-H. Yoon, M.G. Lee, Dynamic modulation of ANO1/TMEM16A HCO₃⁻ permeability by Ca²⁺/calmodulin, *Proc. Natl. Acad. Sci. U. S. A.* 110 (2013) 360–365, <http://dx.doi.org/10.1073/pnas.1211594110>.
- [19] I. Jun, M.H. Cheng, E. Sim, J. Jung, B.L. Suh, Y. Kim, H. Son, K. Park, C.H. Kim, J.-H. Yoon, D.C. Whitcomb, I. Bahar, M.G. Lee, Pore dilatation increases the bicarbonate permeability of CFTR, ANO1 and glycine receptor anion channels, *J. Physiol.* 594 (2016) 2929–2955, <http://dx.doi.org/10.1113/jp271311>.
- [20] R. Schreiber, I. Uliyakina, P. Kongsuphol, R. Warth, M. Mirza, J.R. Martins, K. Kunzelmann, Expression and function of epithelial anoctamins, *J. Biol. Chem.* 285 (2010) 7838–7845, <http://dx.doi.org/10.1074/jbc.M109.065367>.
- [21] X. Jin, S. Shah, Y. Liu, H. Zhang, M. Lees, Z. Fu, J.D. Lippiat, D.J. Beech, A. Sivaprasadarao, S.A. Baldwin, H. Zhang, N. Gamper, Activation of the Cl⁻ channel ANO1 by localized calcium signals in nociceptive sensory neurons requires coupling with the IP₃ receptor, *Sci. Signal.* 6 (2013) ra73, <http://dx.doi.org/10.1126/scisignal.2004184>.
- [22] K. Kunzelmann, TMEM16, LRRC8A, bestrophin: chloride channels controlled by Ca²⁺ and cell volume, *Trends Biochem. Sci.* 40 (2015) 535–543, <http://dx.doi.org/10.1016/j.tibs.2015.07.005>.
- [23] K. Kunzelmann, I. Cabrita, P. Wanitchakool, J. Ousingsawat, L. Sirianant, R. Benedetto, R. Schreiber, Modulating Ca²⁺ signals: a common theme for TMEM16, Ist2, and TMC, *Pflugers Arch. - Eur. J. Physiol.* 468 (2016) 475–490, <http://dx.doi.org/10.1007/s00424-015-1767-4>.
- [24] J.D. Brunner, N.K. Lim, S. Schenck, A. Duerst, R. Dutzler, X-ray structure of a calcium-activated TMEM16 lipid scramblase, *Nature* 516 (2014) 207–212, <http://dx.doi.org/10.1038/nature13984>.
- [25] K. Yu, C. Duran, Z. Qu, Y.-Y. Cui, H.C. Hartzell, Explaining calcium-dependent gating of anoctamin-1 chloride channels requires a revised topology, *Circ. Res.* 110 (2012) 990–999, <http://dx.doi.org/10.1161/CIRCRESAHA.112.264440>.
- [26] H.M. Botelho, I. Uliyakina, N.T. Awatade, M.C. Proença, C. Tischer, L. Sirianant, K. Kunzelmann, R. Pepperkok, M.D. Amaral, Protein traffic disorders: an effective high-throughput fluorescence microscopy pipeline for drug discovery, *Sci. Report.* 5 (2015) 9038, <http://dx.doi.org/10.1038/srep09038>.
- [27] H. Erfle, B. Neumann, P. Rogers, J. Bulkescher, J. Ellenberg, R. Pepperkok, Work flow for multiplexing siRNA assays by solid-phase reverse transfection in multiwell plates, *J. Biomol. Screen.* 13 (2008) 575–580, <http://dx.doi.org/10.1177/1087057108320133>.
- [28] W. Namkung, P.-W. Phuan, A.S. Verkman, TMEM16A inhibitors reveal TMEM16A as a minor component of calcium-activated chloride channel conductance in airway and intestinal epithelial cells, *J. Biol. Chem.* 286 (2011) 2365–2374, <http://dx.doi.org/10.1074/jbc.M110.175109>.
- [29] H. Erfle, B. Neumann, U. Liebel, P. Rogers, M. Held, T. Walter, J. Ellenberg, R. Pepperkok, Reverse transfection on cell arrays for high content screening microscopy, *Nat. Protoc.* 2 (2007) 392–399, <http://dx.doi.org/10.1038/nprot.2006.483>.
- [30] B. Neumann, M. Held, U. Liebel, H. Erfle, P. Rogers, R. Pepperkok, J. Ellenberg, High-throughput RNAi screening by time-lapse imaging of live human cells, *Nat. Methods* 3 (2006) 385–390, <http://dx.doi.org/10.1038/nmeth876>.
- [31] J.C. Simpson, B. Joggerst, V. Laketa, F. Verissimo, C. Cetin, H. Erfle, M.G. Bexiga, V.R. Sigan, J.-K. Hériché, B. Neumann, A. Mateos, J. Blake, S. Bechtel, V. Benes, S. Wiemann, J. Ellenberg, R. Pepperkok, Genome-wide RNAi screening identifies human proteins with a regulatory function in the early secretory pathway, *Nat. Cell Biol.* 14 (2012) 764–774, <http://dx.doi.org/10.1038/ncb2510>.
- [32] J. Almaça, D. Faria, M. Sousa, I. Uliyakina, C. Conrad, L. Sirianant, L.A. Clarke, J.P. Martins, M. Santos, J.K. Herich, W. Huber, R. Schreiber, R. Pepperkok, K. Kunzelmann, M.D. Amaral, High-content siRNA screen reveals global ENaC regulators and potential cystic fibrosis therapy targets, *Cell* 154 (2013), <http://dx.doi.org/10.1016/j.cell.2013.08.045>.
- [33] P. Perez-Cornejo, A. Gokhale, C. Duran, Y. Cui, Q. Xiao, H.C. Hartzell, V. Faundez, Anoctamin 1 (Tmem16A) Ca²⁺-activated chloride channel stoichiometrically interacts with an ezrin-radixin-moesin network, *Proc. Natl. Acad. Sci.* 109 (2012) 10376–10381, <http://dx.doi.org/10.1073/pnas.1200174109>.
- [34] R.D. La Fuente, W. Namkung, Small-molecule screen identifies inhibitors of a human intestinal calcium-activated chloride channel, *Mol. Pharmacol.* 73 (2008) 758–768, <http://dx.doi.org/10.1124/mol.107.043208>.
- [35] W. Namkung, Z. Yao, W.E. Finkbeiner, A.S. Verkman, Small-molecule activators of TMEM16A, a calcium-activated chloride channel, stimulate epithelial chloride secretion and intestinal contraction, *FASEB J.* 25 (2011) 4048–4062, <http://dx.doi.org/10.1096/fj.11-191627>.
- [36] Y. Seo, J. Park, M. Kim, H.K. Lee, J.-H. Kim, J.-H. Jeong, W. Namkung, Inhibition of ANO1/TMEM16A Chloride Channel by Idenobone and its cytotoxicity to cancer cell lines, *PLoS One* 10 (2015) e0133656, <http://dx.doi.org/10.1371/journal.pone.0133656>.
- [37] Y.-S. Lee, Y. Bae, N. Park, J.C. Yoo, C.-H. Cho, K. Ryo, E.M. Hwang, J.-Y. Park, Surface expression of the Anoctamin-1 (ANO1) channel is suppressed by protein-protein interactions with β-COP, *Biochem. Biophys. Res. Commun.* 475 (2016) 216–222, <http://dx.doi.org/10.1016/j.bbrc.2016.05.077>.
- [38] F. Giordano, Y. Saheki, O. Idevall-Hagren, S.F. Colombo, M. Pirruccello, I. Milosevic, E.O. Gracheva, S.N. Bagriantsev, N. Borgese, P. De Camilli, PI(4,5)P₂-dependent and Ca²⁺ - regulated ER-PM interactions mediated by the extended synaptotagmins, *Cell* (2013), <http://dx.doi.org/10.1016/j.cell.2013.05.026>.
- [39] A.G. Manford, C.J. Stefan, H.L. Yuan, J.A. MacGurn, S.D. Emr, ER-to-plasma membrane tethering proteins regulate cell signaling and ER morphology, *Dev. Cell* 23 (2012) 1129–1140, <http://dx.doi.org/10.1016/j.devcel.2012.11.004>.
- [40] C.M. Schauder, X. Wu, Y. Saheki, P. Narayanaswamy, F. Torta, M.R. Wenk, P. De Camilli, K.M. Reinisch, Structure of a lipid-bound extended synaptotagmin indicates a role in lipid transfer, *Nature* 510 (2014) 552–555, <http://dx.doi.org/10.1038/nature13269>.
- [41] M.J. Amaya, A.G. Oliveira, L.K. Schroeder, E.S. Allgeyer, J. Bewersdorf, M.H. Nathanson, Apical localization of inositol 1,4,5-trisphosphate receptors is independent of extended Synaptotagmins in hepatocytes, *PLoS One* 9 (2014) e114043, <http://dx.doi.org/10.1371/journal.pone.0114043>.
- [42] A. Sclip, T. Bacaj, L.R. Giam, T.C. Südhof, Extended Synaptotagmin (ESyt) triple knock-out mice are viable and fertile without obvious endoplasmic reticulum dysfunction, *PLoS One* 11 (2016) e0158295, <http://dx.doi.org/10.1371/journal.pone.0158295>.
- [43] M.G. Tremblay, T. Moss, Loss of all 3 extended Synaptotagmins does not affect normal mouse development, viability or fertility, *Cell Cycle* 15 (2016) 2360–2366, <http://dx.doi.org/10.1080/15384101.2016.1203494>.
- [44] Y. Saheki, X. Bian, C.M. Schauder, Y. Sawaki, M.A. Surma, C. Klose, F. Pincet, K.M. Reinisch, P. De Camilli, Control of plasma membrane lipid homeostasis by the extended synaptotagmins, *Nat. Cell Biol.* 18 (2016), <http://dx.doi.org/10.1038/ncb3339>.
- [45] F. Huang, H. Zhang, M. Wu, H. Yang, M. Kudo, C.J. Peters, P.G. Woodruff, O.D. Solberg, M.L. Donne, X. Huang, D. Sheppard, J.V. Fahy, P.J. Wolters, B.L.M. Hogan, W.E. Finkbeiner, M. Li, Y.-N. Jan, L.Y. Jan, J.R. Rock, Calcium-activated chloride channel TMEM16A modulates mucin secretion and airway smooth muscle contraction, *Proc. Natl. Acad. Sci. U. S. A.* 109 (2012) 16354–16359, <http://dx.doi.org/10.1073/pnas.1214596109>.
- [46] G. Gallos, K.E. Remy, J. Danielsson, H. Funayama, X.W. Fu, H.-Y.S. Chang, P. Yim, D. Xu, C.W. Emala, Functional expression of the TMEM16 family of calcium-activated chloride channels in airway smooth muscle, *Am. J. Physiol. Lung Cell. Mol. Physiol.* 305 (2013) L625–34, <http://dx.doi.org/10.1152/ajplung.00068.2013>.
- [47] C.-H. Zhang, Y. Li, W. Zhao, L.M. Lifshitz, H. Li, B.D. Harfe, M.-S. Zhu, R. ZhuGe, The transmembrane protein 16A Ca²⁺-activated Cl⁻ channel in airway smooth muscle contributes to airway hyperresponsiveness, *Am. J. Respir. Crit. Care Med.* 187 (2013) 374–381, <http://dx.doi.org/10.1164/rccm.201207-1303OC>.
- [48] H. Li, X. Yan, R. Li, A. Zhang, Z. Niu, Z. Cai, W. Duan, X. Li, H. Zhang, Increased TMEM16A involved in alveolar fluid clearance after lipopolysaccharide stimulation, *Inflammation* 39 (2016) 881–890, <http://dx.doi.org/10.1007/s10753-016-0320-8>.